

1 **Prevention of EloR/KhpA heterodimerization by introduction of site-specific amino acid**
2 **substitutions renders the essential elongasome protein PBP2b redundant in *Streptococcus***
3 ***pneumoniae*.**

4 Anja Ruud Winther, Morten Kjos, Gro Anita Stamsås, Leiv Sigve Håvarstein and Daniel
5 Straume*.

6 *The Norwegian University of Life Sciences, Faculty of Chemistry, Biotechnology and Food*
7 *Science, Christian Magnus Falsens vei 1, 1430 Ås, Norway*

8

9 Keywords: *Streptococcus pneumoniae*, elongasome, EloR, KhpA, PBP2b.

10 *Corresponding author: Daniel Straume

11 The Norwegian University of Life Sciences, Faculty of Chemistry, Biotechnology and Food
12 Science, Christian Magnus Falsens vei 1, 1430 Ås, Norway

13 E-mail: daniel.straume@nmbu.no

14 Phone: +47 67 23 25 60

15

16

17 **Abstract.**

18 The RNA binding proteins EloR and KhpA are important components of the regulatory
19 network that controls and coordinates cell elongation and division in *S. pneumoniae*. Loss of
20 either protein reduces cell length, and makes the essential elongasome proteins PBP2b and
21 RodA dispensable. It has been shown previously in formaldehyde crosslinking experiments
22 that EloR co-precipitates with KhpA, indicating that they form a complex *in vivo*. In the present
23 study, we used 3D modeling and site directed mutagenesis in combination with protein
24 crosslinking to further study the relationship between EloR and KhpA. Protein-protein
25 interaction studies demonstrated that KhpA forms homodimers and that KhpA in addition binds
26 to the KH-II domain of EloR. Site directed mutagenesis identified isoleucine 61 (I61) as crucial
27 for KhpA homodimerization. When substituting I61 with phenylalanine, KhpA lost the ability
28 to homodimerize, while it still interacted clearly with EloR. In contrast, both homo- and
29 heterodimerization were lost when I61 was substituted with tyrosine. By expressing these
30 KhpA versions in *S. pneumoniae*, we were able to show that disruption of EloR/KhpA
31 heterodimerization makes the elongasome redundant in *S. pneumoniae*. Of note, loss of KhpA
32 homodimerization did not give rise to this phenotype, demonstrating that the EloR/KhpA
33 complex is crucial for regulating the activity of the elongasome. In support of this conclusion,
34 we found that localization of KhpA to the pneumococcal mid-cell region depends on its
35 interaction with EloR. Furthermore, we found that the EloR/KhpA complex co-localizes with
36 FtsZ throughout the cell cycle.

37

38

39 **Introduction.**

40 In most bacteria, the cytoplasmic membrane is surrounded by a peptidoglycan layer, which
41 gives the cell its shape and provides resistance to internal turgor pressure¹. The peptidoglycan
42 sacculus also serves as an anchoring device for surface proteins and other cell wall components
43 such as teichoic acids and extracellular polysaccharides²⁻⁵. During cell division and growth, the
44 peptidoglycan synthesis machineries add new material into the existing cell wall. In ovoid
45 bacteria, such as the important human pathogen *Streptococcus pneumoniae*, two modes of cell
46 wall synthesis occur. The divisome synthesizes the septal crosswall, while extension of the
47 lateral cell body is carried out by the elongasome^{6,7}. The cell wall synthesis machineries of *S.*
48 *pneumoniae* contain six penicillin binding proteins (PBPs), five of which participate in building
49 the cell wall via transglycosylase and transpeptidase reactions. The class A PBPs, PBP1a,
50 PBP2a, PBP1b, perform both reactions, while the class B PBPs, PBP2b and PBP2x, only have
51 transpeptidase activity. Recently, it was discovered that the monofunctional class B enzymes
52 PBP2x and PBP2b operate in conjunction with FtsW and RodA, two newly discovered
53 transglycosylases belonging to the SEDS family proteins (shape, elongation, division and
54 sporulation)^{8,9}. The sixth PBP, PBP3, is a D,D-carboxypeptidase that reduces the level of inter
55 peptide cross-bridges in the peptidoglycan by cleaving off the C-terminal D-Ala residue in stem
56 pentapeptides¹⁰. PBP2b and RodA have been found to be essential for cell elongation, while
57 PBP2x and FtsW are essential for synthesis of the septal disc. Functional studies and
58 subcellular localizations suggest that PBP2b/RodA and PBP2x/FtsW are key components of
59 the elongasome and the divisome, respectively¹¹⁻¹⁴. It is not clear whether the elongasome- and
60 divisome activities alternate or if these machineries work simultaneously during cell
61 division^{6,15}. However, some data suggest a short period of cell elongation before the onset of
62 septal peptidoglycan synthesis^{12,16}.

63 In contrast to rod-shaped bacteria, *S. pneumoniae* lacks MreB, a cytoskeleton-like
64 protein that moves with the cell wall synthesis machinery in helical patterns perpendicular to
65 the cell length axis¹⁷. Instead, pneumococci elongate by inserting new peptidoglycan into the
66 existing cell wall between the future cell equator and the septum in a circumferentially motion
67 guided by the FtsZ/FtsA division ring^{6,18-21}. At some point during cell elongation, the divisome
68 initiates septal cross wall synthesis. If the coordinated activities of the elongasome and the
69 divisome get out of control, it leads to severe growth defects and development of morphological
70 abnormalities^{11,13,22}. The cells have therefore developed sophisticated systems to monitor cell
71 cycle progression in order to fine-tune the activity of the elongasome and divisome during cell
72 division. One of these systems includes the membrane-spanning eukaryotic-like
73 serine/threonine kinase StkP. It has four extracellular cell-wall-binding PASTA domains,
74 which are believed to monitor the status of the cell wall during division and activate the
75 appropriate cell division proteins through phosphorylation²³⁻²⁶.

76 In a recent study we found that EloR, which is phosphorylated by StkP on threonine
77 89²⁷, is a key regulator of cell elongation in *S. pneumoniae*²⁸. Our results indicated that EloR
78 stimulates cell elongation when phosphorylated, while being inactive or preventing elongation
79 in its non-phosphorylated form. Moreover, we found that $\Delta eloR$ cells can survive without
80 PBP2b and its cognate SEDS transglycosylase RodA, demonstrating that deletion of *eloR*
81 suppresses the need for a functional elongasome in *S. pneumoniae*. Cells lacking EloR displayed
82 a significant reduction in growth rate and became short and round^{28,29}. EloR is a cytoplasmic
83 protein of 37 kDa comprising three different domains: an N-terminal jag-domain of unknown
84 function followed by two RNA-binding domains, a type II KH domain (KH-II) and R3H, at
85 the C-terminal end^{30,31}. In a recent study Zheng et al.³² showed that EloR co-precipitates with
86 a protein called KhpA after treating cells with formaldehyde cross linker. KhpA is a small (8.9
87 kDa) RNA-binding protein that consists only of a type II KH domain. Similar to EloR, deletion

88 of the *khpA* gene supresses the need for a fully functional elongasome, as *pbp2b* as well as
89 *rodA* can be deleted in a $\Delta khpA$ mutant³². EloR and KhpA must bind specific target RNAs
90 probably resulting in modulated expression of cell division proteins during different stages of
91 the cell cycle. In support of this hypothesis Zheng et al.³² reported that the absence of EloR or
92 KhpA results in higher cellular levels of the cell division protein FtsA, and that this increase
93 compensates for the loss of PBP2b³². Homologs of EloR and KhpA appear to be widespread
94 in many Gram-positive bacteria, and are found in genera such as *Streptococcus*, *Bacillus*,
95 *Clostridium*, *Listeria*, *Enterococcus*, *Lactobacillus* and *Lactococcus*. The conservation of these
96 proteins across large phylogenetic distances indicates that they are central players in the cell
97 elongation and division machineries of low G+C Gram-positive bacteria.

98 In the present study, we show that KhpA homodimerizes, and that it in addition interacts
99 with the KH-II domain of EloR forming an EloR/KhpA heterodimer. Furthermore, we
100 identified amino acids critical for these interactions. We successfully constructed a single
101 amino acid mutant of KhpA that fails to homodimerize but still interacts with EloR, and a single
102 amino acid mutant that neither self-interacts nor heterodimerizes. The unique properties of
103 these KhpA versions were used to demonstrate that the function of EloR is compromised when
104 it is no longer able to interact with KhpA, resulting in cells phenocopying $\Delta eloR$ and $\Delta khpA$
105 mutants (reduced cell elongation). Finally, *in vivo* localization studies showed that KhpA co-
106 localizes with FtsZ throughout the cell cycle, and that this localization pattern depends on its
107 interaction with EloR.

108

109

110

111

112 **Results**

113 **Khpa interacts with itself and the KH-II-domain of EloR.**

114 In a recent study we showed that the loss of EloR suppresses the need of a functional
115 elongasome in *S. pneumoniae* since *pbp2b* and *rodA* could be deleted²⁸. Soon after this, Zheng
116 and co-workers published that EloR co-precipitated with a small protein (8.9 kDa) called Khpa
117 in formaldehyde crosslinking experiments. In addition, they found that a $\Delta khpA$ mutant
118 phenocopies a $\Delta eloR$ mutant and that both proteins bound to a similar set of RNA molecules
119 in pulldown experiments³². In the present work, we utilized a bacterial two-hybrid system
120 (BACTH assay) to further study the interaction between EloR and Khpa. The BACTH system
121 is based on interaction-mediated reconstitution of the *Bordetella pertussis* adenylate cyclase
122 CyaA, which consists of two domains (T18 or T25). When brought together through interaction
123 of the proteins tested, the active T18-T25 reconstitution produces cAMP, which ultimately
124 results in measurable β -galactosidase production in the *E. coli* host³³. When testing full-length
125 EloR against Khpa in the BACTH assay, we observed a clear positive interaction (Fig. 1),
126 confirming the crosslinking results of Zheng and co-workers³². Next, we wanted to identify the
127 part of EloR that interacts with Khpa. To do so, each of the three domains of EloR (Jag, KH-
128 II and R3H) was tested individually against Khpa (Fig. 1). The results clearly showed that
129 Khpa specifically interacts with the KH-II-domain of EloR (KH-II^{EloR}).

130 Since KH-domains recognize on average up to four nucleotides, they have a tendency
131 to interact with each other to bind longer sequences and thereby increase their target
132 specificity^{31,34}. We therefore suspected that Khpa self-interacts and forms homodimers.
133 BACTH assays using Khpa fused to T18 and T25 resulted in a positive signal (Fig. 1),
134 suggesting that Khpa, in addition to interacting with EloR, also forms homodimers.

135

136 **Identification of amino acid residues crucial for KhpA homo- and EloR/KhpA**
137 **heterodimerization.**

138 We reasoned that a 3D model of KhpA might help us identify amino acids that are crucial for
139 homodimerization and heterodimerization with EloR. KH-domains have a highly conserved
140 fold and many 3D-structures are available in the databases^{31,34}. To predict the 3D structure of
141 KhpA, we used the online structure prediction tool iTasser. As expected, the predicted structure
142 shows a typical KH-II domain (C-score = -0.36) consisting of three α -helices packed against a
143 three-stranded β -sheet (α - β - β - α - α - β) (Fig. 2A). The conserved RNA binding cleft is made up
144 of the third α -helix and the third β -strand. The typical GxxG loop that interacts with the
145 phosphate backbone of the ssRNA (or in some cases ssDNA) is located between the α 2- and
146 α 3-helices (marked in green in Fig. 2A). Introduction of two aspartates in this loop (GDDG)
147 abolishes binding of target RNA³⁵. To predict the interaction surface between two KhpA
148 molecules, we did protein docking using ZDOCK with the 3D-model of KhpA as input.
149 According to the model (ZDOCK score = 895.421), the α 3-helix creates an anti-parallel
150 interaction surface between two KhpA proteins, resulting in a homodimeric structure where the
151 GxxG loops of the two proteins point in opposite directions (Fig. 2B). Based on this structure,
152 we made four different mutant versions of KhpA in which single amino acids predicted to
153 protrude from the α 3-helix was altered (R53K, R59K, T60Q and I61F). The point mutated
154 versions of KhpA were then tested for their ability to homodimerize by performing BACTH
155 assays. The changes in position 53, 59 or 60 did not dramatically reduce homodimerization,
156 but changing I61 to the bulkier phenylalanine abolished the interaction between KhpA
157 monomers (Fig. 2C). In our 3D model, a bulky phenylalanine in position 61 cannot fit in a
158 dimeric structure due to steric hindrance (Fig. 2B), complying with the loss of
159 homodimerization. The model also shows that R53 locates on opposite sides in a KhpA dimer,
160 while R59 sticks into the RNA binding cavity (see supplemental Fig. S1), which might explain

161 why changing these residues did not give any dramatic effect on dimerization. The T60, on the
162 other hand, appears to be in close contact in a KhpA dimer (Fig. S1), but it seems to be less
163 important for dimerization than I61.

164 To get more accurate data on the effect of the I61F mutation, we chose to measure the
165 β -galactosidase production when performing BACTH (see Materials and Methods). Indeed,
166 the KhpA^{I61F} mutant protein has completely lost the ability to self-interact, but can still form
167 heterodimers with EloR (Fig. 3A). In an attempt to create a KhpA mutant that does not form
168 homodimers nor EloR/KhpA heterodimers, I61 was changed to tyrosine, which adds a polar
169 hydroxyl group to the bulky phenyl ring. When tested in BACTH assays, our results showed
170 that the KhpA^{I61Y} mutant has lost the ability to interact with itself and the interaction with EloR
171 was dramatically reduced (Fig. 3A).

172 Amino acid sequence alignment of the KH-II^{EloR} domain and KhpA, suggests that
173 leucine 239 (L239) in EloR corresponds to I61 in KhpA (see supplemental Fig. S2).
174 Accordingly, when L239 in EloR was substituted with a tyrosine, KhpA could no longer
175 interact with EloR^{L239Y}, showing that this residue is indeed important for EloR/KhpA
176 heterodimerization (Fig. 3A). To prove that L239 and I61 are in close proximity in the
177 EloR/KhpA heterodimer, we replaced these two amino acids with cysteins to determine
178 whether this would result in a disulfide bridge between the two proteins *in vivo*. A
179 pneumococcal strain expressing the mutant proteins EloR^{L239C} and KhpA^{I61C} was therefore
180 constructed (strain AW336). EloR^{L239C} contained an N-terminal 3xflag-tag to allow detection
181 with α -flag antibodies. Strain AW336 was grown to exponential phase, harvested, and lysed
182 using SDS loading buffer with or without the reducing agent β -mercaptoethanol (see Material
183 and Methods). Next, samples were analyzed by SDS-PAGE followed by immunoblotting. In
184 non-reduced cell lysates, we detected a shift in band size corresponding to the complex between
185 EloR and KhpA (Fig. 3B). This shift was not present in samples where β -mercaptoethanol had

186 been added to break the disulfide bond, or in any of the samples containing wild type 3xflag-
187 EloR or 3xflag-EloR^{L239C} only. This confirms the interaction between KhpA and the KH-II
188 domain of EloR *in vivo*, and that I61 in the α 3-helix of KhpA interacts directly with L239 in
189 the α 3-helix of the KH-II^{EloR} domain.

190

191 **Prevention of EloR/KhpA heterodimerization relieves the requirement of *pbp2b*.**

192 A $\Delta khpA$ mutant phenocopies a $\Delta eloR$ mutant³². Both mutants have reduced growth rates, form
193 shorter cells and are viable without a functional elongasome (i.e. without a *pbp2b* or *rodA*
194 gene)^{28,32}. We hypothesized that the reason why $\Delta khpA$ cells phenocopies $\Delta eloR$ cells is
195 because deletion of either will prevent the formation of the EloR/KhpA complex. In other
196 words, the elongasome only becomes essential when the EloR/KhpA complex is able to form
197 and carry out its normal biological function. To test this hypothesis we exploited the unique
198 properties of KhpA^{I61F} and KhpA^{I61Y}. KhpA^{I61F} does not form homodimers, but form
199 heterodimers with EloR, while KhpA^{I61Y} is unable to form either. First, we examined if
200 expression of KhpA^{I61F} or KhpA^{I61Y} generated cells with reduced growth rate similar to a
201 $\Delta khpA$ mutant. Deletion of *khpA* (strain DS420) increased the doubling time with
202 approximately 15 minutes, which complies with previous findings (15-30 minutes)³², while
203 strains expressing KhpA^{I61F} or KhpA^{I61Y} (AW212 and AW275) had growth rates similar to the
204 wild type strain (data not shown). Microscopic examination of KhpA^{I61F} or KhpA^{I61Y} cells
205 showed that the KhpA^{I61Y} strain grew in short chains similar to KhpA deficient cells. The
206 KhpA^{I61F} strain on the other hand grew mainly as diplococci similar to the wild type strain (Fig.
207 4A). By measuring cell lengths and widths, it became evident that KhpA^{I61Y} cells, in which
208 KhpA is unable to form a complex with EloR, have a rounder cell morphology with reduced
209 cell elongation similar to $\Delta khpA$ cells (Fig. 4B). This phenotype is also characteristic for $\Delta eloR$

210 cells^{28,29,32}. In contrast, cells expressing the monomeric version of KhpA (I61F) that can still
211 form a complex with EloR, displayed a normal length/width distribution (Fig. 4B).

212 To further test our hypothesis that EloR/KhpA heterodimerization is required for
213 normal elongasome function, we compared pneumococcal mutants expressing KhpA^{I61F},
214 KhpA^{I61Y} and EloR^{L239Y} (AW279) with respect to the essentiality of their *pbp2b* gene. Indeed,
215 *pbp2b* could be deleted in KhpA^{I61Y} and EloR^{L239Y} cells with normal transformation
216 frequencies, but not in KhpA^{I61F} cells (see Table S1). Deletion of *pbp2b* in these strains could
217 not be attributed to decreased stability of the mutated EloR and KhpA version since
218 immunodetection of Flag-tagged EloR^{L239Y}, KhpA^{I61F} and KhpA^{I61Y} showed that they were
219 expressed at similar levels as the wild type proteins (see Fig. S4). Since it has been shown that
220 mutants expressing a KhpA unable to bind ssRNA (changing the ssRNA-binding motif GxxG
221 to GDDG) have a $\Delta khpA/\Delta eloR$ phenotype³², we wondered whether this was because
222 KhpA^{GDDG} had reduced interaction with EloR. However, our BACTH assay showed that
223 KhpA^{GDDG} successfully formed a complex with EloR (Fig. 4C), and we confirmed that *pbp2b*
224 could be deleted in pneumococci expressing KhpA^{GDDG}, as also reported by Zheng et al³². This
225 demonstrates that PBP2b becomes redundant in cells having an EloR/KhpA complex in which
226 KhpA no longer binds RNA or when KhpA no longer interacts with EloR.

227

228 **EloR recruits KhpA to the division site.**

229 KhpA and EloR have been shown to co-localize to the septal region of dividing cells^{28,32}. Since
230 they form heterodimers *in vivo*, we wondered if KhpA is recruited to mid-cell through its
231 interaction with EloR. To explore this, the subcellular localization of sfGFP-fused KhpA
232 (KhpA-sfGFP was functional since *pbp2b* could not be deleted in strain AW5, see Table S1)
233 was determined in wild type cells and in a $\Delta eloR$ mutant (Fig. 5). A subtle mid-cell enrichment

234 of KhpA-sfGFP was found in 73.2% of wild type cells, confirming previous findings³². In
235 contrast, KhpA-sfGFP was found at mid-cell in only 0.5% of the $\Delta eloR$ mutant cells. To show
236 that it is the direct interaction between KhpA and EloR that localizes KhpA to the division site
237 and not some indirect effect of deleting the *eloR* gene, we fused sfGFP to KhpA^{I61F} and
238 KhpA^{I61Y}. As expected, KhpA^{I61Y}-sfGFP, which does not bind EloR, lost its localization to
239 mid-cell (found at mid-cell in only 2% of the cells). The monomeric KhpA^{I61F}-sfGFP are still
240 able to interact with EloR and displayed significantly higher degree of mid-cell enrichment
241 (found at mid-cell in 19% of the cells). In accordance with these results, expression of
242 EloR^{L239Y}, which cannot interact with KhpA, resulted in mislocalization of KhpA-sfGFP (Fig.
243 5). Together, these results show that KhpA is recruited to mid-cell through complex formation
244 with EloR.

245 To determine whether the EloR/KhpA complex is recruited to the division zone during
246 early, late or all stages of cell division, we compared the localization patterns of KhpA and
247 FtsZ. FtsZ forms the division ring, which functions as a scaffold for a number of proteins found
248 in the elongasome and divisome. FtsZ is therefore present at the division zone during initiation
249 of new septa, cell elongation and cross wall synthesis, but it is not required for the final stage
250 of daughter cell separation^{12,18}. KhpA-sfGFP and FtsZ fused to the fluorescent marker mKate2
251 were co-expressed in *S. pneumoniae* (strain AW198), and fluorescence microscopy images
252 demonstrate that KhpA-sfGFP enriched at mid-cell follows the same localization pattern as
253 FtsZ (Fig. 6). This shows that the EloR/KhpA complex is recruited to the division zone at the
254 very early stage, and that it remains co-localized with the cell division machineries throughout
255 the cell cycle. Note, however, that KhpA is not exclusively co-localized with FtsZ as it is also
256 found throughout the cytoplasm.

257

258 **Discussion.**

259 It has been shown previously that $\Delta khpA$ and $\Delta eloR$ mutant strains are similar in several
260 respects. They both exhibit reduced cell lengths, and are able to survive without PBP2b and
261 other essential components of the elongasome^{28,32}. The fact that $\Delta khpA$ and $\Delta eloR$ mutants
262 have similar phenotypes could suggest that KhpA and EloR are acting at different steps in the
263 same regulatory pathway. However, the finding that KhpA co-precipitates with EloR after
264 formaldehyde crosslinking³² suggests an alternative model, namely that they function as a
265 single unit and that disruption of this complex gives rise to the phenotypes described above.
266 The results presented in the present work prove that the latter model is correct. Disruption of
267 the EloR/KhpA complex by introduction of site-specific amino acid substitutions, gives rise to
268 shorter cells and renders the elongasome redundant (Fig. 7). It is therefore likely that its role is
269 to stimulate or control elongasome-mediated lateral cell wall synthesis. To do this, our results
270 show that KhpA must be able to bind its target nucleic acid, which is most likely ssRNA. The
271 typical binding surface of KH-domains can only accommodate four unpaired bases^{31,34}, and
272 consequently has low binding specificity. It is reasonable to assume that the RNA sequence
273 motifs recognized by KhpA and the KH-II domain of EloR are different. Hence, by combining
274 the two domains in a heterodimer the binding specificity and affinity for its target ssRNA(s)
275 are substantially increased. Another possible role for the interaction between EloR and KhpA
276 could be to bridge two segments on an RNA molecule by binding two distant motifs, inducing
277 a loop formation. Such loops are proposed to facilitate binding of posttranscriptional regulatory
278 protein complexes^{34,36,37}. Identification of the EloR/KhpA RNA target(s) will be an important
279 goal for future research seeking to understand the function of the EloR/KhpA system.

280 Our results show that KhpA also forms homodimers, which might have their own
281 distinct biological function (see Fig. 1 and 3A). However, our preliminary studies did not detect
282 any obvious functional deficits or major phenotypic changes associated with the KhpA^{I61F}

283 mutation, i.e. the mutation disrupting the formation of KhpA homodimers without preventing
284 the formation of EloR/KhpA heterodimers. As the docking model shows, the KhpA monomers
285 are likely arranged in an antiparallel orientation in the dimer so that they will be able bind two
286 successive sequence motifs on the same RNA strand. The binding of two motifs will increase
287 the target sequence specificity considerably, and will make the RNA sequence motif
288 recognized by the homodimer different from that recognized by the EloR/KhpA heterodimer.
289 Considering this, and that the KhpA^{I61F} and KhpA^{I61Y} mutations give rise to completely
290 different phenotypes, it is likely that the KhpA homodimers and EloR/KhpA heterodimers
291 serve different biological functions.

292 The EloR/KhpA heterodimer contains three RNA-binding domains, i.e two domains
293 from EloR (KH-II and R3H) and one from KhpA. The presence of several RNA-binding
294 domains is a common feature of proteins containing KH-domains. As mentioned above, this
295 increases target specificity and is also believed to have an important role in the folding of
296 ssRNA sequences³⁴. Based on the present and previous studies^{28,29,32}, we know that the
297 EloR/KhpA complex requires the combined action of all three RNA-binding domains to
298 regulate cell elongation. However, it is not known whether all three domains bind to the same
299 RNA strand, or if the KH-II^{EloR}/KhpA complex binds one strand while the R3H domain binds
300 another. The crystal structure of an EloR homolog from *Clostridium symbiosum* (PDB 3GKU)
301 suggests a dimeric structure³⁸, which in principle could bind two KhpA molecules resulting in
302 a complex with a total of six RNA-binding domains. To test this possibility we used the
303 BACTH system to determine if EloR from *S. pneumoniae* forms homodimers. The results were
304 inconclusive as we obtained just a weak positive signal (data not shown). Hence, we cannot
305 conclude whether the biologically active complex between EloR and KhpA is dimeric
306 (EloR/KhpA) or tetrameric (KhpA/EloR/EloR/KhpA).

307 Synthesis of the lateral cell wall takes place in an area close to the division septum,
308 possibly where the division septum meets the periphery of the cell. Previous studies show that
309 EloR and KhpA localize to the septal region^{28,32}. Here, we show that KhpA homodimers are
310 found throughout the cytoplasm (strain AW353) (Fig. 5), while KhpA/EloR heterodimers
311 localize together with FtsZ to the division site (AW198) (Fig. 6). This finding support the
312 notion that these homo- and heterodimers serve different functions. Of note, FtsZ has been
313 reported to disappear from the septum prior to both essential cell division proteins PBP2x
314 (divisome) and PBP2b (elongasome)¹². Since KhpA co-localizes with the FtsZ-ring throughout
315 the cell cycle, it suggests that a functional EloR/KhpA complex is important during the stages
316 of cell division, which involves active peptidoglycan synthesis during cell elongation and early
317 to mid crosswall synthesis, but not during the final stage of cell division.

318 Zheng and co-workers report that the levels of FtsA, which together with FtsZ
319 assembles into the division ring^{6,18,39,40}, were elevated two- to threefold in $\Delta eloR$ and $\Delta khpA$
320 mutants. Their results suggest that EloR and KhpA bind 5' untranslated regions of mRNAs,
321 including the *ftsA* transcript, resulting in altered translation rates³². In support of this hypothesis
322 they found that *pbp2b* could be deleted in wild type D39 cells overexpressing FtsA, although
323 overexpression of FtsA could not fully restore the wild type phenotype of $\Delta eloR/\Delta khpA$ cells³².
324 We attempted to reproduce the described effect of elevated FtsA levels in our D39 strain.
325 However, despite using the exact same expression conditions, i.e. overexpression of *ftsA* and
326 its 24 nt upstream region from a P_{Zn} zinc-inducible promoter, we were not successful.
327 Nevertheless, translational control of specific mRNAs seems to be the most probable mode of
328 action for the EloR/KhpA complex.

329 Interestingly, the *eloR* gene is co-transcribed with a gene called *yidC* in *S. pneumoniae*⁴¹
330 and most likely in several other bacteria including *S. thermophilus*, *L. monocytogenes*, *B.*
331 *subtilis*, *L. lactis*, *E. faecium* and *L. plantarum*. Such conserved co-transcription could indicate

332 a functional relationship between the genes. YidC is an insertase that assists in co-translational
333 insertion of membrane proteins into the lipid bilayer. It functions together with the SecYEG
334 translocon, the signal recognition particle (SRP) and the SRP-receptor FtsY. During co-
335 translational protein targeting to the SecYEG translocon, the SRP-ribosome-nascent protein
336 chain complex is first targeted to FtsY, which delivers the chain to the SecYEG translocon
337 channel. The function of YidC is to facilitate the release of the transmembrane domains of
338 inner membrane proteins from the channel into the lipid bilayer^{42,43}. Having this in mind, it is
339 tempting to speculate that the EloR/KhpA complex could be involved in regulating the
340 expression and insertion of specific membrane proteins involved in cell elongation through
341 translational control.

342

343 **Methods.**

344 **Bacterial strains, cultivation and transformation**

345 All strains used in this work are listed in Table 1. *E. coli* strains were grown in LB broth at
346 37°C with shaking (200 rpm), or on LB plates at 37°C unless otherwise indicated. When
347 necessary the following antibiotics were used: kanamycin (50 µg/ml) and ampicillin (100
348 µg/ml). Transformation experiments were performed with chemically competent cells using
349 the heat shock method at 42°C for 45 seconds. *S. pneumoniae* were grown in C medium⁴⁴ or
350 on Todd Hewitt-agar plates at 37°C. Agar plates were incubated in anaerobic chambers using
351 AnaeroGen[™] bags from Oxoid. When necessary, kanamycin (400 µg/ml) and streptomycin
352 (200 µg/ml) were employed for selection of transformants. In order to knock out genes or
353 introduce mutations, natural genetic transformation was employed. For transformation
354 experiments, the culture was grown to an OD₅₅₀ of 0.05-0.1 and mixed with the transforming
355 DNA (100-200 ng) and CSP1, which was added to a final concentration of 250 ng/ml. After 2

356 hours of incubation at 37°C, 30 µl of the culture was plated on TH-agar containing the
357 appropriate antibiotic followed by incubation at 37°C over night. To investigate growth rates
358 of different mutants, cultures were grown to an OD₅₅₀ of 0.2, diluted to OD₅₅₀ = 0.05, and
359 grown in 96-well Corning NBS clear-bottom plates in a Synergy H1 Hybrid Reader (BioTek).
360 The OD₅₅₀ was measured automatically every 5 minutes for 20 hours.

361

362 **Construction of genetic mutants, gene fusions and point mutations**

363 DNA amplicons used in transformation experiments were created with overlap extension PCR
364 as previously described⁴⁵. Genes were knocked out using a Janus cassette⁴⁶. The cassettes were
365 created with sequences of ~1000 bp homologous to the flanking sequences of the insertion site
366 in the genome. The same technique was employed when introducing point mutations or fusion
367 genes. Primers used to create these amplicons are listed in Table S2. The *ftsZ*-mKate2 fusion
368 gene together with a kanamycin resistance cassette was amplified from genomic DNA of strain
369 RR66⁴⁷. All constructs were verified with PCR and Sanger Sequencing.

370 **SDS-PAGE and immunoblotting**

371 The strains RH425, SPH448, AW334 and AW336 were grown to an OD₅₅₀ of 0.3 in a culture
372 volume of 45 ml. The cells were harvested at 4000 x g, and resuspended in 200 µl 1 x SDS
373 sample buffer not containing any reducing agents. The samples were then split in two, and β-
374 mercaptoethanol was added to one parallel half of the samples to a final concentration of 100
375 mM. All the samples (including the non-reduced) were heated at 100 °C for 10 minutes. The
376 cell lysates were separated on a 15 % polyacrylamide gel with buffer conditions as previously
377 described⁴⁸. For immunodetection purposes, the separated proteins were electroblotted onto a
378 PVDF membrane (BioRad), and flag-EloR was detected with α-flag antibodies as previously
379 described⁴⁹. To detect the expression of Flag-EloR, Flag-EloR^{L239Y}, Flag-KhpA, Flag-KhpA^{I61F}

380 and Flag-KhpA^{I61Y}, strain SPH448, DS766, AW9, DS764 and DS765 were grown to OD₅₅₀ =
381 0.3 in 10 ml C medium. Flag-tagged proteins were then detected in whole cell lysates as
382 described above.

383 **BACTH-assay**

384 The bacterial adenylate cyclase two hybrid (BACTH) assay, is based on the functional
385 complementation of T18 and T25, two domains of the *B. pertussis* adenylate cyclase (CyaA)³³.
386 When these domains are brought in close proximity to each other, they can actively produce
387 cAMP. The production of cAMP leads to activation of the catabolite activator protein CAP,
388 which in a complex with cAMP activates expression of a reporter gene placed behind the
389 cAMP/CAP promoter. The reporter gene used in this system encodes the β -galactosidase
390 enzyme. In order to investigate the interaction between two proteins, we cloned genes encoding
391 the proteins of interest in frame with either the T25 -or the T18-encoding sequences in plasmids
392 provided by the manufacturer (Euromedex). The plasmids used in this study are listed in Table
393 S3. Next, two plasmids, each expressing one protein fused to either T18 or T25 were
394 transformed into *E. coli* BTH101 cells (a *cya*⁻ strain). After overnight incubation on LB plates
395 containing kanamycin (50 μ g/ml) and ampicillin (100 μ g/ml), five colonies from each
396 transformation were grown in LB containing the appropriate antibiotics. When reaching an
397 OD₆₀₀ of 0.2, three μ l of the cell cultures were spotted onto LB plates containing 0.5 mM IPTG
398 (to induce expression of the fusion genes), X-gal (40 μ g/ml), kanamycin (50 μ g/ml) and
399 ampicillin (100 μ g/ml). After an overnight incubation at 30°C, results were interpreted as
400 positive or negative based on the color of the spot. A positive interaction between the proteins
401 of interest will result in blue spots on a plate. In addition, the production of β -galactosidase
402 reporter was measured by performing β -galactosidase assays using ortho-nitrophenyl- β -
403 galactoside (ONPG) as substrate. *E. coli* BTH101 containing plasmids with T18 and T25-fused
404 genes were grown in the presence of kanamycin (50 μ g/ml) and ampicillin (100 μ g/ml) to

405 OD₆₀₀ = 0.4-0.5. Then the cells were diluted to OD₆₀₀ = 0.05 in similar medium also containing
406 0.5 mM IPTG. The cells were incubated at 30 °C with shaking for 4 hours. Cells from one ml
407 culture were lysed using 0.5 g of ≤106 μm glass beads (Sigma) and bead beating at 6.5 m/s for
408 3x20 seconds. Then the β-galactosidase activity in 100 μl cell lysate was determined following
409 the protocol of Steinmoen *et al.*⁵⁰.

410 **Microscopy and cell shape distribution analyses**

411 The subcellular localization of different point mutated versions of the KhpA proteins was
412 examined by fluorescence microscopy. The mutated proteins in question were fused to sfGFP⁴⁷
413 via a short glycine-linker (GGGGG). sfGFP fusions were expressed in the native *khpA* locus
414 in the *S. pneumoniae* genome (strains AW5, AW198, AW238, AW267, AW321 and AW353).

415 The cell morphology and cell shape distributions were examined by phase contrast
416 microscopy. Microscopy experiments were performed by growing the strains to an OD₅₅₀ of
417 0.1 before immobilizing the cells on a microscopy slide using 1.2 % low melting agarose
418 (Biorad) in PBS. Phase contrast images and GFP fluorescence images were obtained using a
419 Zeiss AxioObserver with ZEN Blue software, and an ORCA-Flash 4.0 V2 Digital CMOS
420 camera (Hamamatsu Photonics) using a 1003 phase-contrast objective. The ImageJ plugin
421 MicrobeJ⁵¹ was used to analyze the cell shape and the subcellular localization of KhpA-sfGFP
422 and FtsZ-mKate2. Cells were segmented using the phase contrast images. Cell shape
423 distributions were made by calculating length/width for the individual cell and the significance
424 of the differences between distributions were determined using a two-sample t-test. To
425 determine the percentage of cells having KhpA-sfGFP enriched at mid-cell, the GFP
426 fluorescence profiles were plotted for the individual cells. KhpA-sfGFP was scored as mid-cell
427 localized when a fluorescence maximum peak was found in the mid-cell area (between 40-60
428 % of the cell length), and the percentage of cells with KhpA-sfGFP enriched at mid-cell was

429 calculated. To analyze the subcellular localization of FtsZ-mKate2 and KhpA-sfGFP, the
430 Maxima-option in MicrobeJ was used.

431 **3D-modelling**

432 The online structure determination tool iTasser was used to predict the 3D-structure of KhpA.
433 It uses algorithms to predict protein 3D structure based on the amino acid sequence and known,
434 published structures⁵². KhpA was modeled based on the solved structure of the KH-II domain
435 of PDB entry 3gku (21% sequence identity and 60% similarity with KhpA). The ZDOCK
436 server was used to predict the interaction surface in a KhpA homodimer⁵³. Based on the
437 predicted interaction surface in a KhpA homodimer, we created point mutated versions of
438 KhpA, introduced these into the BACTH system, and tested interactions between mutated
439 KhpA proteins and between mutated KhpA and wild type EloR.

440

441 **Acknowledgements.**

442 This work was partly funded by a grant given by the Research Council of Norway.

443

444 **Authors Contributions.**

445 A.R.W. made mutants strains, performed BACTH assays, microscopy and immunoblots. M.K.
446 performed microscopy, cell shape measurements and revised the manuscript. G.A.S. helped
447 with constructing mutant strains, interpreting results and revising the manuscript. L.S.H.
448 contributed with experimental design, 3D-modelling, interpreting results and revising the
449 manuscript. D.S. contributed with experimental design, BACTH assays, interpreting results
450 and writing of the manuscript.

451

452 **Additional information.**

453 The authors have no financial competing interests or conflict of interests regarding the data
454 presented in this study.

455

456 **References.**

- 457 1 Vollmer, W., Blanot, D. & de Pedro, M. A. Peptidoglycan structure and architecture.
458 *FEMS Microbiol Rev* **32**, 149-167, doi:10.1111/j.1574-6976.2007.00094.x (2008).
- 459 2 Dramsi, S., Magnet, S., Davison, S. & Arthur, M. Covalent attachment of proteins to
460 peptidoglycan. *FEMS Microbiol Rev* **32**, 307-320, doi:10.1111/j.1574-
461 6976.2008.00102.x (2008).
- 462 3 Brown, S., Santa Maria, J. P., Jr. & Walker, S. Wall teichoic acids of gram-positive
463 bacteria. *Annu Rev Microbiol* **67**, 313-336, doi:10.1146/annurev-micro-092412-
464 155620 (2013).
- 465 4 Bazaka, K., Crawford, R. J., Nazarenko, E. L. & Ivanova, E. P. Bacterial extracellular
466 polysaccharides. *Adv Exp Med Biol* **715**, 213-226, doi:10.1007/978-94-007-0940-9_13
467 (2011).
- 468 5 Sørensen, U. B., Henrichsen, J., Chen, H. C. & Szu, S. C. Covalent linkage between the
469 capsular polysaccharide and the cell wall peptidoglycan of *Streptococcus pneumoniae*
470 revealed by immunochemical methods. *Microb Pathog* **8**, 325-334 (1990).
- 471 6 Pinho, M. G., Kjos, M. & Veening, J. W. How to get (a)round: mechanisms controlling
472 growth and division of coccoid bacteria. *Nature reviews. Microbiology* **11**, 601-614,
473 doi:10.1038/nrmicro3088 (2013).

- 474 7 Zapun, A., Vernet, T. & Pinho, M. G. The different shapes of cocci. *FEMS Microbiol*
475 *Rev* **32**, 345-360, doi:10.1111/j.1574-6976.2007.00098.x (2008).
- 476 8 Cho, H. *et al.* Bacterial cell wall biogenesis is mediated by SEDS and PBP polymerase
477 families functioning semi-autonomously. *Nat Microbiol*, 16172,
478 doi:10.1038/nmicrobiol.2016.172 (2016).
- 479 9 Meeske, A. J. *et al.* SEDS proteins are a widespread family of bacterial cell wall
480 polymerases. *Nature* **537**, 634-638, doi:10.1038/nature19331 (2016).
- 481 10 Morlot, C. *et al.* Crystal structure of a peptidoglycan synthesis regulatory factor (PBP3)
482 from *Streptococcus pneumoniae*. *J Biol Chem* **280**, 15984-15991,
483 doi:10.1074/jbc.M4084446200 (2005).
- 484 11 Berg, K. H., Stamsås, G. A., Straume, D. & Håvarstein, L. S. Effects of low PBP2b
485 levels on cell morphology and peptidoglycan composition in *Streptococcus*
486 *pneumoniae* R6. *J Bacteriol* **195**, 4342-4354, doi:10.1128/JB.00184-13 (2013).
- 487 12 Tsui, H. C. *et al.* Pbp2x localizes separately from Pbp2b and other peptidoglycan
488 synthesis proteins during later stages of cell division of *Streptococcus pneumoniae* D39.
489 *Mol Microbiol* **94**, 21-40, doi:10.1111/mmi.12745 (2014).
- 490 13 Land, A. D. *et al.* Requirement of essential Pbp2x and GpsB for septal ring closure in
491 *Streptococcus pneumoniae* D39. *Mol Microbiol* **90**, 939-955, doi:10.1111/mmi.12408
492 (2013).
- 493 14 Perez-Nunez, D. *et al.* A new morphogenesis pathway in bacteria: unbalanced activity
494 of cell wall synthesis machineries leads to coccus-to-rod transition and filamentation in
495 ovococci. *Mol Microbiol* **79**, 759-771, doi:10.1111/j.1365-2958.2010.07483.x (2011).
- 496 15 Sham, L. T., Tsui, H. C., Land, A. D., Barendt, S. M. & Winkler, M. E. Recent advances
497 in pneumococcal peptidoglycan biosynthesis suggest new vaccine and antimicrobial
498 targets. *Curr Opin Microbiol* **15**, 194-203, doi:10.1016/j.mib.2011.12.013 (2012).

- 499 16 Wheeler, R., Mesnage, S., Boneca, I. G., Hobbs, J. K. & Foster, S. J. Super-resolution
500 microscopy reveals cell wall dynamics and peptidoglycan architecture in ovococcal
501 bacteria. *Mol Microbiol* **82**, 1096-1109, doi:10.1111/j.1365-2958.2011.07871.x (2011).
- 502 17 Garner, E. C. *et al.* Coupled, circumferential motions of the cell wall synthesis
503 machinery and MreB filaments in *B. subtilis*. *Science* **333**, 222-225,
504 doi:10.1126/science.1203285 (2011).
- 505 18 Mura, A. *et al.* Roles of the essential protein FtsA in cell growth and division in
506 *Streptococcus pneumoniae*. *J Bacteriol*, doi:10.1128/JB.00608-16 (2016).
- 507 19 Jacq, M. *et al.* Remodeling of the Z-Ring Nanostructure during the *Streptococcus*
508 *pneumoniae* cell cycle revealed by photoactivated localization microscopy. *MBio* **6**,
509 doi:10.1128/mBio.01108-15 (2015).
- 510 20 Fleurie, A. *et al.* Interplay of the serine/threonine-kinase StkP and the paralogs DivIVA
511 and GpsB in pneumococcal cell elongation and division. *PLoS Genet* **10**, e1004275,
512 doi:10.1371/journal.pgen.1004275 (2014).
- 513 21 Li, Y. *et al.* MapZ forms a stable ring structure that acts as a nanotrack for FtsZ
514 treadmilling in *Streptococcus mutans*. *ACS Nano*, doi:10.1021/acsnano.8b02469
515 (2018).
- 516 22 Straume, D., Stamsås, G. A., Berg, K. H., Salehian, Z. & Håvarstein, L. S. Identification
517 of pneumococcal proteins that are functionally linked to penicillin-binding protein 2b
518 (PBP2b). *Mol Microbiol* **103**, 99-116, doi:10.1111/mmi.13543 (2017).
- 519 23 Fleurie, A. *et al.* Mutational dissection of the S/T-kinase StkP reveals crucial roles in
520 cell division of *Streptococcus pneumoniae*. *Mol Microbiol* **83**, 746-758,
521 doi:10.1111/j.1365-2958.2011.07962.x (2012).

- 522 24 Novakova, L. *et al.* Identification of multiple substrates of the StkP Ser/Thr protein
523 kinase in *Streptococcus pneumoniae*. *J Bacteriol* **192**, 3629-3638,
524 doi:10.1128/JB.01564-09 (2010).
- 525 25 Beilharz, K. *et al.* Control of cell division in *Streptococcus pneumoniae* by the
526 conserved Ser/Thr protein kinase StkP. *Proc Natl Acad Sci U S A* **109**, E905-913,
527 doi:10.1073/pnas.1119172109 (2012).
- 528 26 Zucchini, L. *et al.* PASTA repeats of the protein kinase StkP interconnect cell
529 constriction and separation of *Streptococcus pneumoniae*. *Nat Microbiol* **3**, 197-209,
530 doi:10.1038/s41564-017-0069-3 (2018).
- 531 27 Sun, X. *et al.* Phosphoproteomic analysis reveals the multiple roles of phosphorylation
532 in pathogenic bacterium *Streptococcus pneumoniae*. *J Proteome Res* **9**, 275-282,
533 doi:10.1021/pr900612v (2010).
- 534 28 Stamsås, G. A. *et al.* Identification of EloR (Spr1851) as a regulator of cell elongation
535 in *Streptococcus pneumoniae*. *Mol Microbiol* **105**, 954-967, doi:10.1111/mmi.13748
536 (2017).
- 537 29 Ulrych, A. *et al.* Characterization of pneumococcal Ser/Thr protein phosphatase *phpP*
538 mutant and identification of a novel PhpP substrate, putative RNA binding protein Jag.
539 *BMC Microbiol* **16**, 247, doi:10.1186/s12866-016-0865-6 (2016).
- 540 30 Grishin, N. V. The R3H motif: a domain that binds single-stranded nucleic acids.
541 *Trends Biochem Sci* **23**, 329-330 (1998).
- 542 31 Valverde, R., Edwards, L. & Regan, L. Structure and function of KH domains. *FEBS J*
543 **275**, 2712-2726, doi:10.1111/j.1742-4658.2008.06411.x (2008).
- 544 32 Zheng, J. J., Perez, A. J., Tsui, H. T., Massidda, O. & Winkler, M. E. Absence of the
545 KhpA and KhpB (JAG/EloR) RNA-binding proteins suppresses the requirement for

546 PBP2b by overproduction of FtsA in *Streptococcus pneumoniae* D39. *Mol Microbiol*
547 **106**, 793-814, doi:10.1111/mmi.13847 (2017).

548 33 Karimova, G., Pidoux, J., Ullmann, A. & Ladant, D. A bacterial two-hybrid system
549 based on a reconstituted signal transduction pathway. *Proc Natl Acad Sci USA* **95**,
550 5752-5756 (1998).

551 34 Nicastro, G., Taylor, I. A. & Ramos, A. KH-RNA interactions: back in the groove. *Curr*
552 *Opin Struct Biol* **30**, 63-70, doi:10.1016/j.sbi.2015.01.002 (2015).

553 35 Hollingworth, D. *et al.* KH domains with impaired nucleic acid binding as a tool for
554 functional analysis. *Nucleic acids research* **40**, 6873-6886 (2012).

555 36 Chao, J. A. *et al.* ZBP1 recognition of beta-actin zipcode induces RNA looping. *Genes*
556 *Dev* **24**, 148-158, doi:10.1101/gad.1862910 (2010).

557 37 Patel, V. L. *et al.* Spatial arrangement of an RNA zipcode identifies mRNAs under post-
558 transcriptional control. *Genes Dev* **26**, 43-53, doi:10.1101/gad.177428.111 (2012).

559 38 Tan, K., Keigher, L., Jedrzejczak, R., Babnigg, G. & Joachimiak, A.
560 (<http://www.rcsb.org/structure/3GKU>).

561 39 Bisson-Filho, A. W. *et al.* Treadmilling by FtsZ filaments drives peptidoglycan
562 synthesis and bacterial cell division. *Science* **355**, 739-743,
563 doi:10.1126/science.aak9973 (2017).

564 40 Yang, X. *et al.* GTPase activity-coupled treadmilling of the bacterial tubulin FtsZ
565 organizes septal cell wall synthesis. *Science* **355**, 744-747,
566 doi:10.1126/science.aak9995 (2017).

567 41 Slager, J., Aprianto, R. & Veening, J. W. Deep genome annotation of the opportunistic
568 human pathogen *Streptococcus pneumoniae* D39. *Nucleic Acids Res*
569 <https://doi.org/10.1093/nar/gky725>, doi:10.1093/nar/gky725 (2018).

570 42 Wu, Z. C., de Keyzer, J., Berrelkamp-Lahpor, G. A. & Driessen, A. J. Interaction of
571 *Streptococcus mutans* YidC1 and YidC2 with translating and nontranslating ribosomes.
572 *J Bacteriol* **195**, 4545-4551, doi:10.1128/JB.00792-13 (2013).

573 43 Steinberg, R., Knupffer, L., Origi, A., Asti, R. & Koch, H. G. Co-translational protein
574 targeting in bacteria. *FEMS Microbiol Lett* **365**, doi:10.1093/femsle/fny095 (2018).

575 44 Lacks, S. & Hotchkiss, R. D. A study of the genetic material determining an enzyme
576 activity in pneumococcus. *Biochimica et Biophysica Acta* **39**, 508-518 (1960).

577 45 Higuchi, R., Krummel, B. & Saiki, R. A general method of in vitro preparation and
578 specific mutagenesis of DNA fragments: study of protein and DNA interactions.
579 *Nucleic acids research* **16**, 7351-7367 (1988).

580 46 Sung, C., Li, H., Claverys, J. & Morrison, D. An *rpsL* cassette, janus, for gene
581 replacement through negative selection in *Streptococcus pneumoniae*. *Applied and*
582 *Environmental Microbiology* **67**, 5190-5196 (2001).

583 47 van Raaphorst, R., Kjos, M. & Veening, J. W. Chromosome segregation drives division
584 site selection in *Streptococcus pneumoniae*. *Proc Natl Acad Sci U S A* **114**, E5959-
585 E5968, doi:10.1073/pnas.1620608114 (2017).

586 48 Laemmli, U. K. Cleavage of structural proteins during the assembly of the head of
587 bacteriophage T4. *nature* **227**, 680 (1970).

588 49 Stamsås, G. A., Straume, D., Salehian, Z. & Håvarstein, L. S. Evidence that
589 pneumococcal WalkK is regulated by StkP through protein–protein interaction.
590 *Microbiology* **163**, 383-399 (2017).

591 50 Steinmoen, H., Knutsen, E. & Håvarstein, L. S. Induction of natural competence in
592 *Streptococcus pneumoniae* triggers lysis and DNA release from a subfraction of the cell
593 population. *Proc Natl Acad Sci USA* **99**, 7681-7686 (2002).

594 51 Ducret, A., Quardokus, E. M. & Brun, Y. V. MicrobeJ, a tool for high throughput
595 bacterial cell detection and quantitative analysis. *Nature Microbiology* **1**, 16077 (2016).

596 52 Roy, A., Kucukural, A. & Zhang, Y. I-TASSER: a unified platform for automated
597 protein structure and function prediction. *Nature Protocols* **5**, 725 (2010).

598 53 Pierce, B. G. *et al.* ZDOCK server: interactive docking prediction of protein–protein
599 complexes and symmetric multimers. *Bioinformatics* **30**, 1771-1773 (2014).

600 54 Johnsborg, O. & Håvarstein, L. S. Pneumococcal LytR, a protein from the LytR-CpsA-
601 Psr family, is essential for normal septum formation in *Streptococcus pneumoniae*. *J*
602 *Bacteriol* **191**, 5859-5864, doi:10.1128/JB.00724-09 (2009).

603

604

606 Table 1. *S. pneumoniae* strains used in the present study.

Name	Relevant characteristics	Reference
R704	R6 derivative, <i>comA::ermAM</i> ; Ery ^R	JP. Claverys* 54
RH425	R704, but streptomycin resistant; Ery ^R , Sm ^R	
DS420	$\Delta comA$, $\Delta khpA$; Ery ^R , Sm ^R	This work
DS428	$\Delta comA$, $\Delta khpA$, $\Delta pbp2b::janus$; Ery ^R , Kan ^R	This work
DS764	$\Delta comA$, <i>flag-khpA</i> ^{I61F} ; Ery ^R , Sm ^R	This work
DS765	$\Delta comA$, <i>flag-khpA</i> ^{I61Y} ; Ery ^R , Sm ^R	This work
DS766	$\Delta comA$, <i>flag-eloR</i> ^{L239Y} ; Ery ^R , Sm ^R	This work
AW5	$\Delta comA$, <i>khpA-sfgfp</i> ; Ery ^R , Sm ^R	This work
AW9	$\Delta comA$, <i>flag-khpA</i> ; Ery ^R , Sm ^R	This work
AW24	$\Delta comA$, <i>khpA</i> ^{GDDG} ; Ery ^R , Sm ^R	This work
AW27	$\Delta comA$, <i>khpA</i> ^{GDDG} , $\Delta pbp2b::janus$; Ery ^R , Kan ^R	This work
AW198	$\Delta comA$, <i>khpA-sfgfp</i> , <i>ftsZ-mKate2-Km</i> ; Ery ^R , Km ^R , Sm ^R	This work
AW212	$\Delta comA$, <i>khpA</i> ^{I61F} ; Ery ^R , Sm ^R	This work
AW238	$\Delta comA$, <i>khpA-sfgfp</i> , $\Delta eloR$; Ery ^R , Sm ^R	This work
AW267	$\Delta comA$, <i>khpA</i> ^{I61F} - <i>sfgfp</i> ; Ery ^R , Sm ^R	This work
AW275	$\Delta comA$, <i>khpA</i> ^{I61Y} ; Ery ^R , Sm ^R	This work
AW279	$\Delta comA$, <i>eloR</i> ^{L239Y} ; Ery ^R , Sm ^R	This work
AW313	$\Delta comA$, <i>khpA</i> ^{I61Y} , $\Delta pbp2b::janus$; Ery ^R , Kan ^R	This work
AW314	$\Delta comA$, <i>eloR</i> ^{L239Y} , $\Delta pbp2b::janus$; Ery ^R , Kan ^R	This work
AW321	$\Delta comA$, <i>khpA</i> ^{I61Y} - <i>sfgfp</i> ; Ery ^R , Sm ^R	This work
AW334	$\Delta comA$, <i>flag-eloR</i> ^{L239C} ; Ery ^R , Sm ^R	This work
AW336	$\Delta comA$, <i>flag-eloR</i> ^{L239C} , <i>khpA</i> ^{I61C} ; Ery ^R , Sm ^R	This work
AW353	$\Delta comA$, <i>khpA-sfgfp</i> , <i>eloR</i> ^{L239Y} ; Ery ^R , Sm ^R	This work
SPH445	$\Delta comA$, $\Delta eloR$, Ery ^R , Sm ^R	28
SPH446	$\Delta comA$, $\Delta eloR$, $\Delta pbp2b::janus$; Ery ^R , Kan ^R	28
SPH448	$\Delta comA$, <i>flag-eloR</i> ; Ery ^R , Sm ^R	28
RR66	D39 derivative, <i>ftsZ-mKate2</i> , Kan ^R	47

607 *Gift from Professor Jean-Pierre Claverys, CNRS, Toulouse, France.

608 **Figure legends**

609 **Fig. 1.** BACTH-assay showing that KhpA interacts directly with EloR and with itself. KhpA
610 (orange shape) was probed against full-length EloR, the R3H domain, the KH-II^{EloR} domain,
611 the Jag domain and EloR missing the C-terminal R3H domain (EloR^{ΔR3H}) (blue shapes).
612 Positive interactions (blue spots) were only seen between KhpA and parts of EloR having the
613 KH-II^{EloR} domain. The positive self-interaction of KhpA is shown at the bottom.

614

615 **Fig. 2.** Structure prediction of KhpA using iTasser and ZDOCK. A. KhpA was predicted to
616 have the typical α - β - β - α - α - β fold of KH-II domains, with the I61 (shown in magenta)
617 protruding from the α 3-helix. B. (upper) Protein-protein docking of KhpA homodimers using
618 ZDOCK. The α 3-helix of two KhpA molecules are predicted to make contact anti-parallel of
619 each other forming a homodimer where the GXXG RNA-binding loops (shown in green) point
620 in opposite directions. The I61 (magenta) of two KhpA monomers are brought in close
621 proximity in the dimeric structure, facilitating a hydrophobic contact surface. (lower) The
622 dimeric model of the I61F substitution suggests that the phenyl ring does not fit properly into
623 the space between the two KhpA molecules probably because this space is occupied by Tyr63
624 (yellow) and Ser64 (cyan) of the other KhpA molecule. C. BACTH assay showing KhpA's
625 ability to form homodimers when selected amino acids in the α 3-helix were changed (R53K,
626 R59K, T60Q and I61F). Positive interactions appear as blue spots.

627

628 **Fig. 3.** The α 3-helix of KhpA is critical for self-dimerization and for EloR/KhpA complex
629 formation. A. Measurements of β -galactosidase production in BACTH assays testing the
630 interaction between EloR and KhpA, KhpA^{I61F} or KhpA^{I61Y} in addition to EloR^{L239Y} against

631 KhpA (green bars). β -galactosidase production resulting from homodimerization of KhpA,
632 KhpA^{I61F} and KhpA^{I61Y} is represented by orange bars, while negative and positive controls are
633 shown in grey. B. Immunoblot detection of 3xflag-EloR in strain RH425, SPH448, AW334
634 and AW336. A Crosslinked EloR/KhpA complex was observed in strain AW336 under non-
635 reducing conditions, but not after reduction with β -mercaptoethanol (+ BME). The image is
636 cropped from the full-length immunoblot, which is shown in Fig. S3.

637

638 **Fig. 4.** A. Comparison of the morphology of strain RH425 (wt), DS420 ($\Delta khpA$), AW212
639 (I61F) and AW275 (I61Y). Loss of KhpA homodimerization (KhpA^{I61F}) produced cells with
640 morphology similar to wild type. Cells in which KhpA no longer interacts with EloR
641 (KhpA^{I61Y}) had morphologies resembling the $\Delta khpA$ mutant. The microscopy images are
642 representatives of whole cell populations. Scale bars are 2 μ m. B. Comparison of the cell-shape
643 distribution (length/width) of $\Delta khpA$ -, KhpA^{I61F}- and KhpA^{I61Y}-cells (in green) with wild type
644 cells (in grey). KhpA^{I61Y} and $\Delta khpA$ cells were both significantly different from wild type
645 ($p < 0.05$, two-sample t-test), while the shape distribution of KhpA^{I61F} cells was similar to wild
646 type. C. Quantitative BACTH assay showing that KhpA^{GDDG} self-dimerizes and forms complex
647 with EloR.

648

649 **Fig. 5.** Micrographs showing the localization of KhpA-sfGFP in strain AW5 (wt), AW238
650 ($\Delta eloR$), AW267 (KhpA^{I61F}-sfGFP), AW321 (KhpA^{I61Y}-sfGFP) and AW353 (EloR^{L239Y}). The
651 percent of cells having KhpA-sfGFP enriched to mid-cell are indicated. Scale bars are 2 μ m.

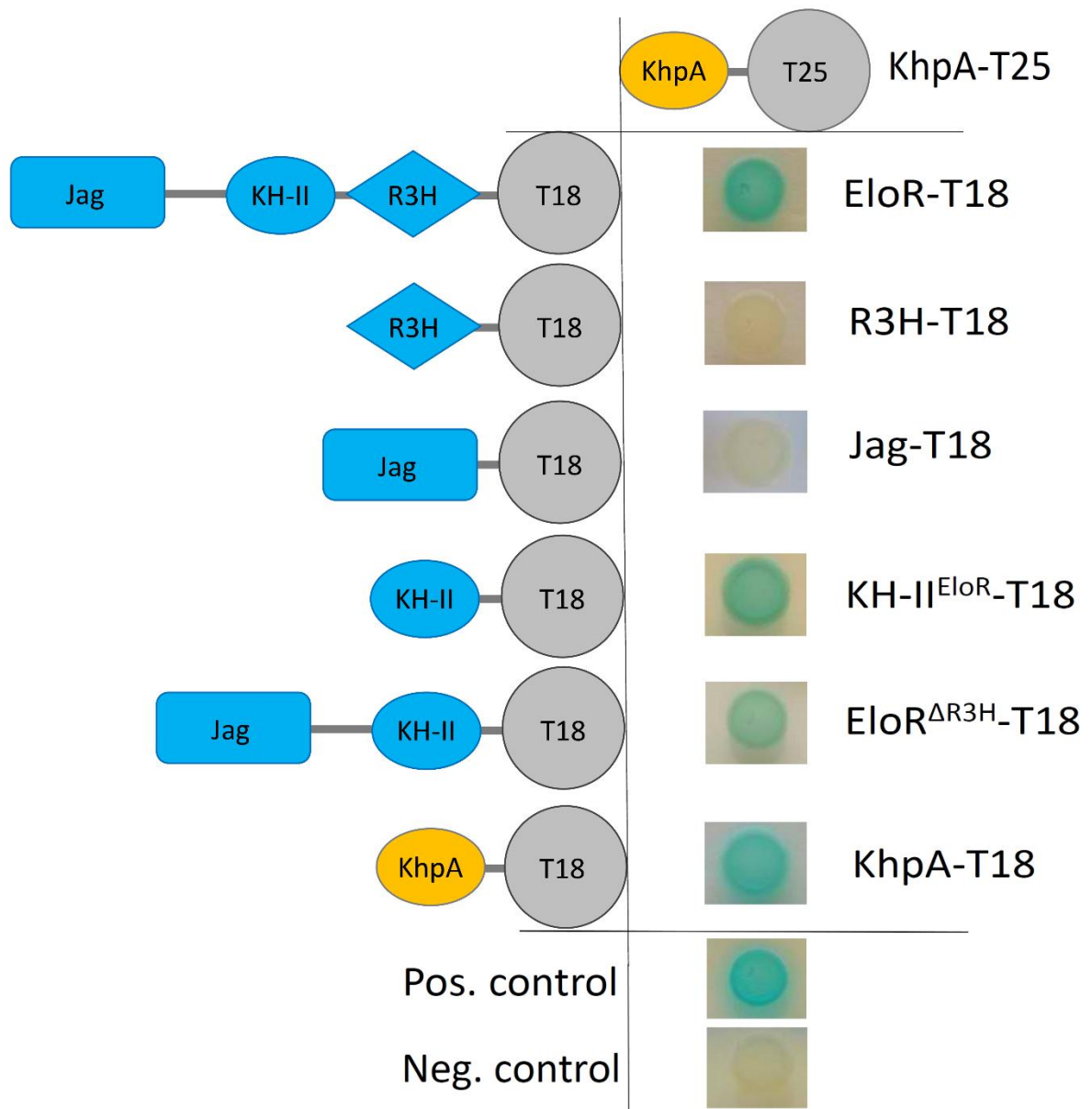
652

653 **Fig. 6.** Localization of KhpA-sfGFP and mKate2-FtsZ at different stages of cell division. A.
654 Microscopic examination of strain AW198 showed that KhpA-sfGFP co-localizes to the
655 division site with FtsZ-mKate2 during cell division. Scale bars are 2 μ m. B. The fluorescence
656 maximum signals of FtsZ-mKate2 and KhpA-sfGFP plotted relative to cell length. 437 cells
657 were analyzed.

658 **Fig. 7.** Model depicting EloR- and KhpA dependent cell elongation. KhpA binds the KH-II
659 domain of EloR, which recruits KhpA to the division zone where new cell wall is synthesized.
660 At the division zone the EloR/KhpA complex regulates cell elongation by binding RNA.
661 Whether EloR/KhpA binds one or more specific sequence motifs or specific RNA secondary
662 structures, and how binding of RNA regulates cell division are still not settled. A monomeric
663 KhpA does not render cells independent on PBP2b as long as it still forms a complex with
664 EloR. If the interaction between EloR and KhpA is broken, KhpA loses its mid-cell localization
665 and binding to the target RNA(s) is most probably reduced or lost. Since EloR requires the
666 RNA binding activity of KhpA to function, preventing EloR/KhpA complex formation results
667 in compromised cell elongation.

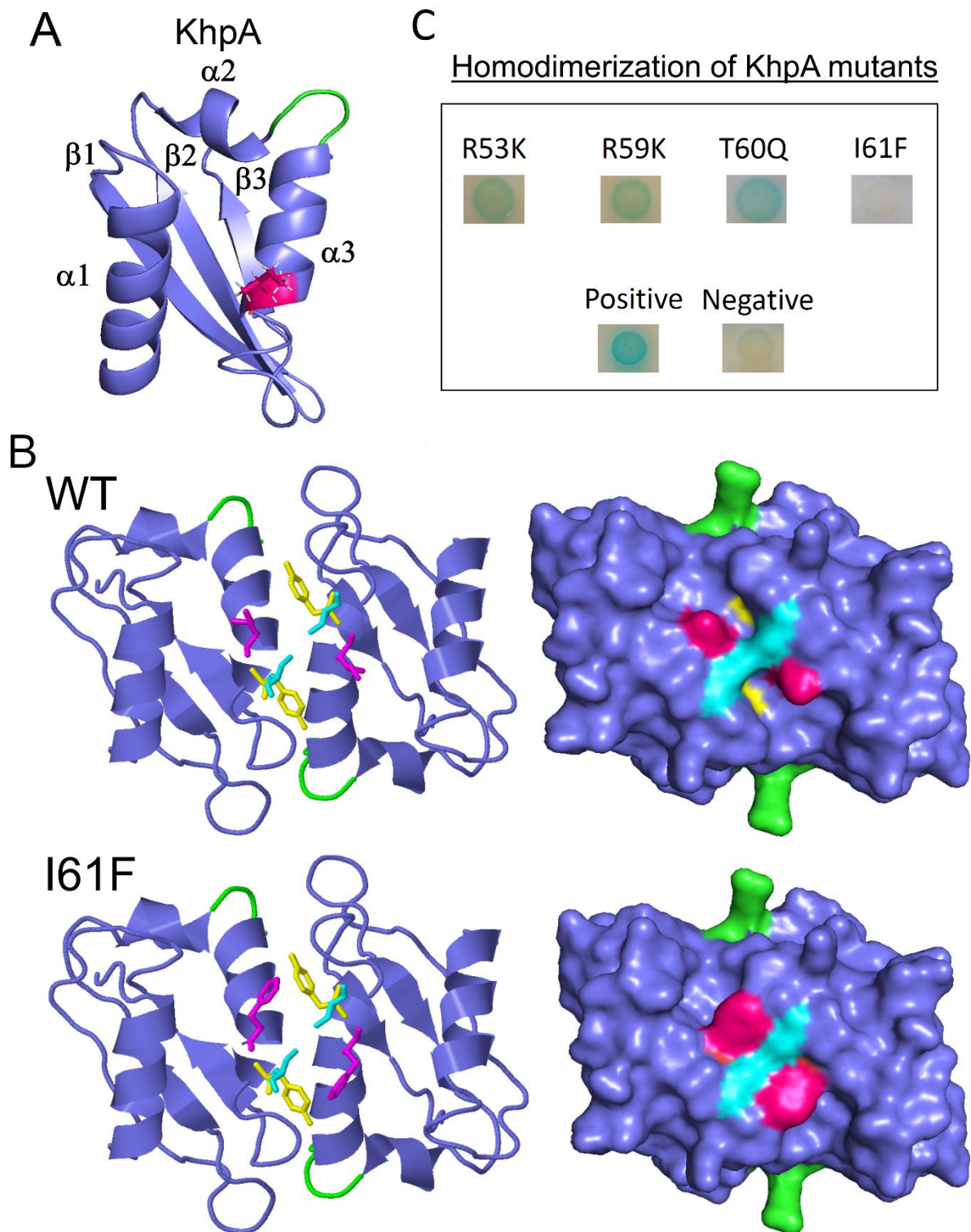
668

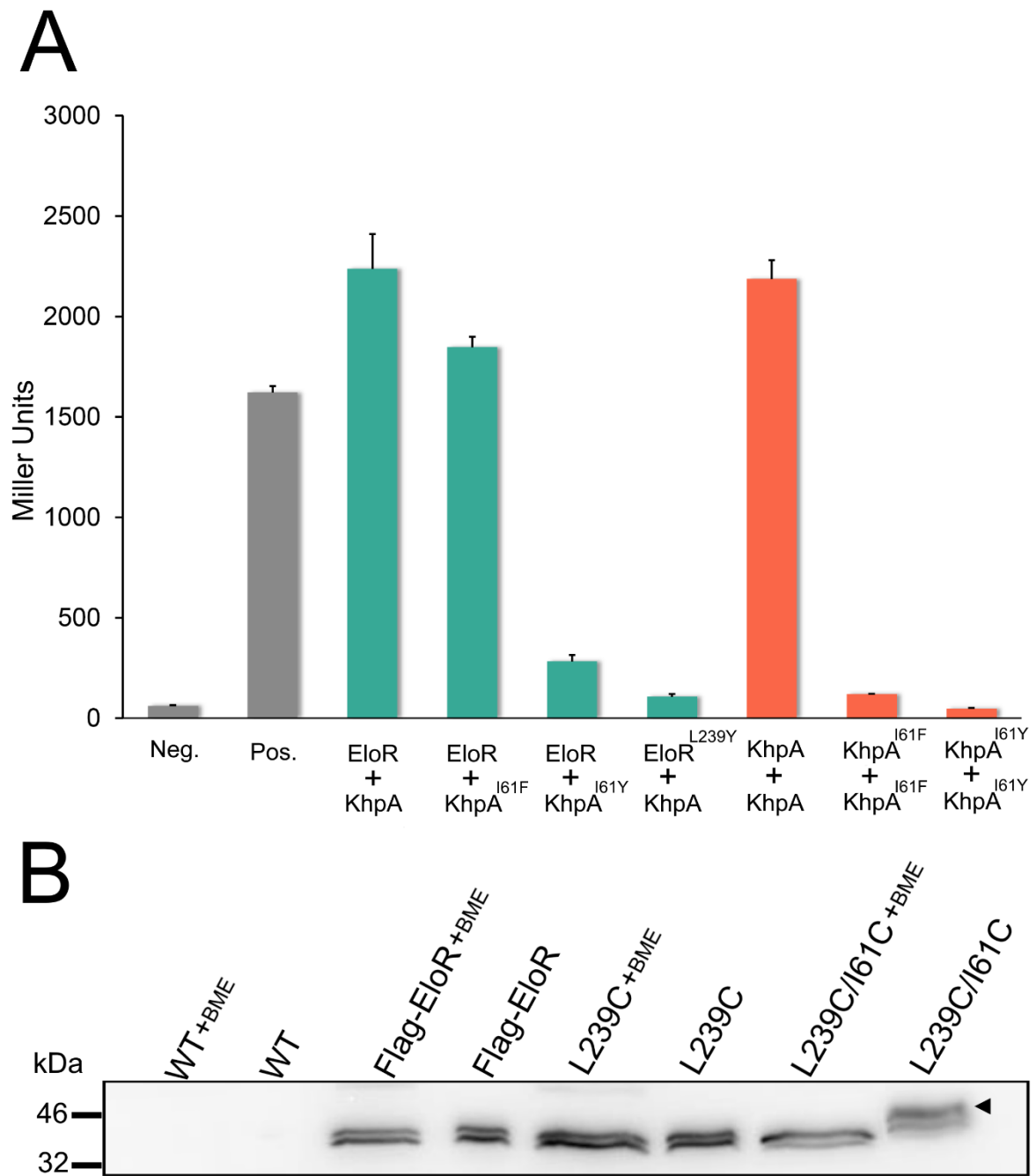
669 Fig. 1.



670

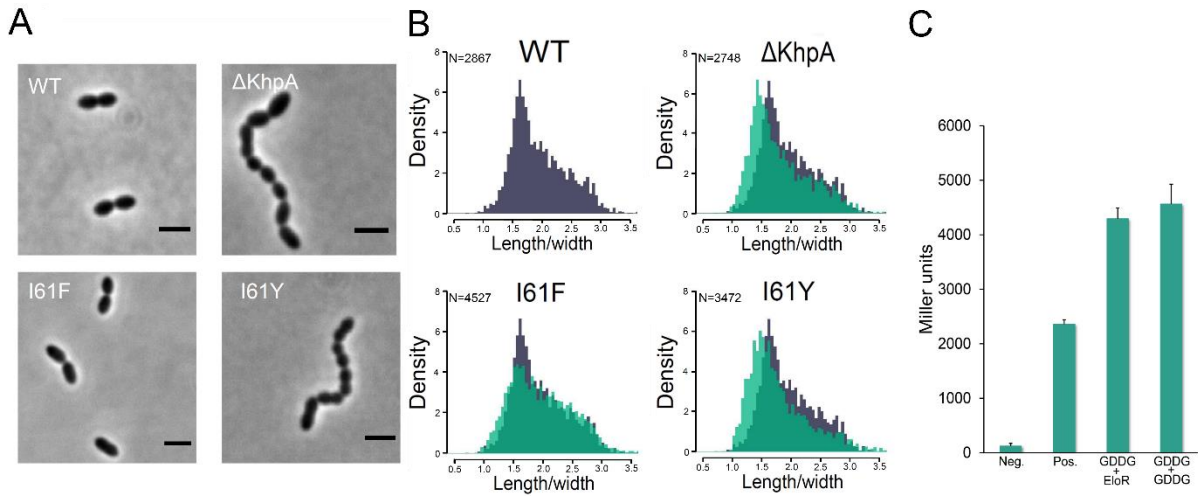
671





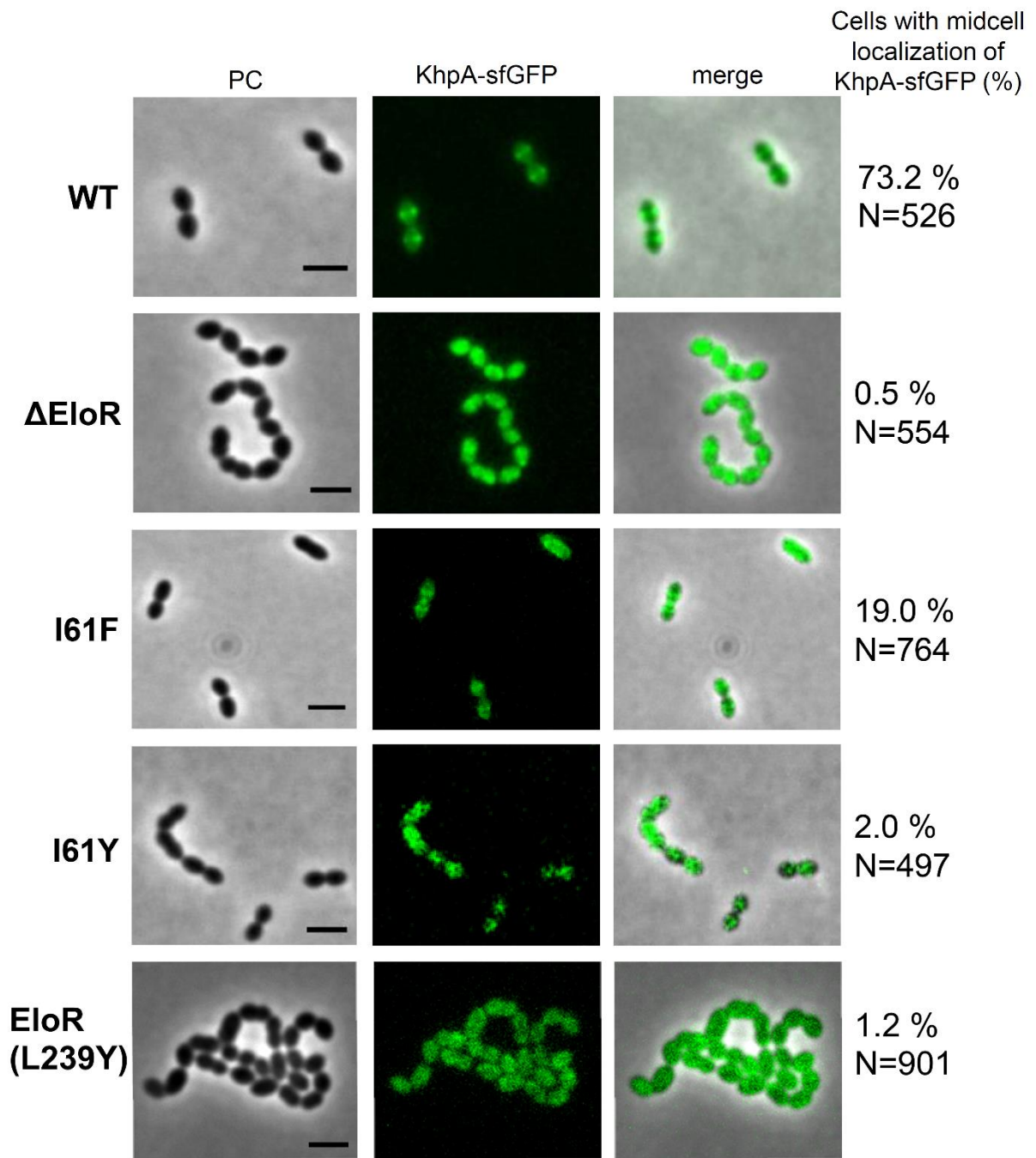
676

677



679

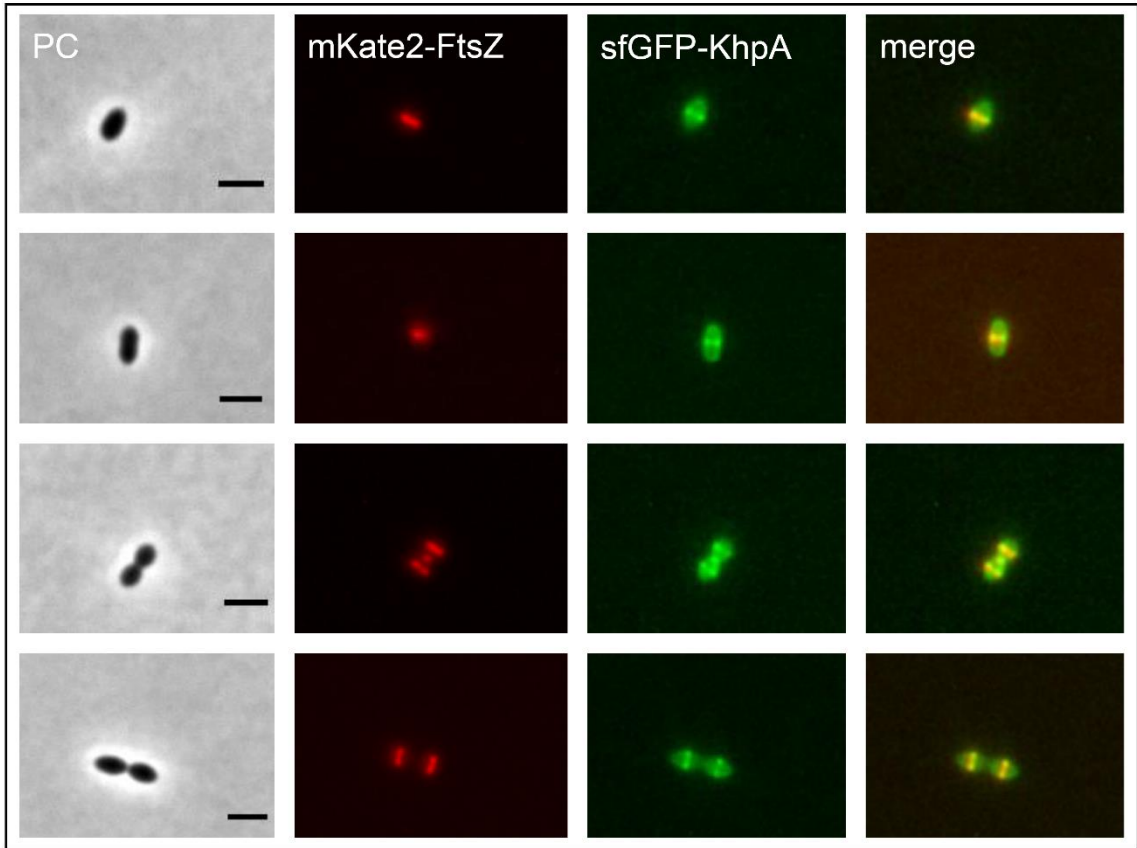
680



682

683

A



B

